Mechanics of Advanced Composite Structures 3 (2016) 123-135

Semnan University

Mechanics of Advanced Composite Structures

journal homepage: http://MACS.journals.semnan.ac.ir

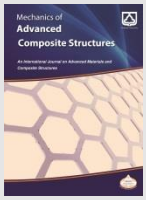

Static and Free Vibration Analyses of Functionally Graded Nanocomposite Plates Reinforced by Wavy Carbon Nanotubes Resting on a Pasternak Elastic Foundation

R. Moradi Dastjerdi [a*], G. Payganeh [b], S. Rajabizadeh Mirakabad [b], M. Jafari Mofrad-Taheri [b]

[a] *Young Researchers and Elite Club,Khomeinishahr Branch, Islamic Azad University, Khomeinishahr, Iran*
[b] *School of Mechanical Engineering, Shahid Rajaee Teacher Training University (SRTTU), Tehran, Iran*

PAPER INFO

Paper history:
Received: 2016-05-27
Revised: 2016-07-23
Accepted: 2016-08-26

Keywords:
Static
Free vibration
Wavy carbon nanotube
Nanocomposite plates
Mesh-Free

ABSTRACT

In this study, static and free vibration analyses of functionally graded (FG) nanocomposite plates, reinforced by wavy single-walled carbon nanotubes (SWCNTs) resting on a Pasternak elastic foundation, were investigated based on a mesh-free method and modified first-order shear deformation theory (FSDT). Three linear types of FG nanocomposite plate distributions and a uniform distribution of wavy carbon nanotubes (CNTs) were considered, in addition to plate thickness. The mechanical properties were by an extended rule of mixture. In the mesh-free analysis, moving least squares (MLS) shape functions were used for approximation of the displacement field in the weak form of a motion equation, and the transformation method was used for imposition of essential boundary conditions. Effects of geometric dimensions, boundary conditions, the type of applied force, and the waviness index, aspect ratio, volume fraction, and distribution pattern of CNTs were examined for their effects on the static and frequency behaviors of FG carbon nanotube reinforced composite (CNTRC) plates. Waviness and the distribution pattern of CNTs had a significant effect on the mechanical behaviors of FG-CNTRC plates, even more than the effect of the CNT volume fraction.

1. Introduction

The extraordinary and outstanding characteristics of carbon nanotubes (CNTs) have broadly attracted researchers' attention since their discovery in the 1990s [1]. Conventional fiber-reinforced composite materials are normally made of stiff and strong fillers with microscale diameters embedded into various matrix phases. The discovery of CNTs may lead to a new ways to improve the properties of the resulting composites by the changing reinforcement phases for nano-scaled fillers [2]. Carbon nanotubes are considered as a potential candidate for the reinforcement of polymer composites, which provide a good interfacial bonding between CNTs and the polymer, and proper dispersion of the individual CNTs in the polymeric matrix can be guaranteed [3]. The CNT/polymer structures may also be supported by an elastic foundation. These kinds of plates are mainly used in concrete roads, rafts, and mat foundations for buildings, and reinforced concrete pavements for airport runways. To describe the interaction between the plate and the foundation, various kinds of foundation models have been proposed. The simplest one is the Winkler or one-parameter model, which regards the foundation as a series of separated springs without coupling effects between them. This model was improved by Pasternak by adding a shear spring to simulate the interactions between the separated springs in the Winkler model. The Pasternak model is widely-used to describe the mechanical behavior of structure-foundation interactions [4].

* Corresponding author, Tel.: +98-913-2058928; Fax: +98-31 -33660088

E-mail address: rasoul.moradi@iaukhsh.ac.ir

On the other hand, the mechanical properties of CNTRCs decrease if the volume fraction of CNTs rises beyond certain limit [5]. Therefore, due to the high cost of CNTs, the modeling of CNTRCs incorporates the concept of functionally graded materials (FGMs) to effectively and efficiently make use of the CNTs. FGMs are classified as novel composite materials with gradient compositional variation. The concept of FGMs can be utilized for the management of a material's microstructure, so that the mechanical behavior of a structure made of such materials can be improved. The composites, which are reinforced by CNTs with grading distribution, are called functionally graded carbon nanotube reinforced composites (FG-CNTRCs). Several works on FG-CNTRC structures were carried out in the wake of new research using FGMs. For example, Shen [6, 7] suggested that the interfacial bonding strength could be improved through the use of a graded distribution of CNTs within the matrix. He examined post-buckling and the nonlinear bending behavior of FG-CNTRC cylindrical shells and plates, respectively, and demonstrated that the linear FG reinforcements can increase the material's mechanical behaviors. Zhu et al. [8] evaluated bending and performed free vibration analyses of thin-to-moderately thick FG-CNTRC plates, using the finite element method (FEM) based on the first-order shear deformation theory (FSDT). Centered on a three-dimensional theory of elasticity, Alibeigloo [9] discussed static analysis of FG-CNTRC plates imbedded in piezoelectric layers using three cases of CNT distribution. Malekzadeh et al. [10] studied the free vibration behaviors of quadrilateral laminated thin-to-moderately-thick FG-CNTRC plates, using the FSDT and the differential quadrature method (DQM). Alibeigloo and Liew [11] presented the bending behaviors of FG-CNTRC rectangular plates with simply supported edges, subjected to thermo-mechanical loads based on a three-dimensional theory of elasticity. Moradi-Dastjerdi et al. [12] used the Navier method and a refined plate theory to investigate the free vibration analysis of simply supported sandwiched plates with FG-CNTRC face sheets resting on a Pasternak elastic foundation. They used straight and randomly oriented CNTs in the FG-CNTRC face sheets.

In addition, some forms of mesh-free methods were used to analyze FG-CNTRC structures. For example, Moradi-Dastjerdi et al. [13-14] presented static and dynamic analyses of FG nanocomposite cylinders reinforced by straight CNTs carried out by a mesh-free method based on an MLS shape function. Additionally, they reported the effects of orientation and aggregation of CNTs on the axisymmetric natural frequencies of FG-nanocomposite cylinders. In this work, they used the Eshelby–Mori–Tanaka approach to estimate the mechanical properties [15]. Lie et al. [16] studied free vibration analysis of FG-CNTRC plates, using the element-free *kp*-Ritz method based on FSDT. Finally, in two related works, Zhang et al. [17, 18] used an element-free based improved moving least squares-Ritz (IMLS-Ritz) method and FSDT to study the buckling behaviors of FG-CNTRC plates resting on a Winkler foundation and the nonlinear bending of the same type of plates resting on a Pasternak elastic foundation.

In all the above-mentioned studies concerning FG-CNTRC structures, they assumed that the CNTs were straight and did not consider the effects of the CNT aspect ratios or waviness, while CNT curvature (waviness index) and CNT aspect ratios dramatically decreased the modulus of elasticity. However, some researchers have studied the effects of FG-CNTRC structures. For example, Martone et al. [19] presented the reinforcement effects of CNTs with different aspect ratios in an epoxy matrix. They showed that progressive reduction of the nanotubes' effective aspect ratios occurred because of the increasing connectedness between the nanotubes with an increase in their concentration. In addition, they investigated the effects of nanotube curvature on the average contact number between tubes by means of the waviness that accounts for the deviation from straight particles' assumptions.

Based on a three-dimensional theory of elasticity, Jam et al. [20] investigated the effects of CNTs aspect ratios and waviness on the vibrational behavior of nanocomposite cylindrical panels, and their results indicated that the distribution pattern and volume fraction of CNTs have a significant effect on the natural frequencies of nanocomposite cylindrical panels. Moradi-Dastjerdi et al. [21, 22] also studied the effects of CNTs' waviness and aspect ratios on the vibrational and dynamic behaviors of FG-CNTRC cylinders. They used a new version for the rule of mixture to show the effect of CNT waviness on the reinforcement behaviors of the nanocomposites. They considered different distribution patterns and waviness conditions with variable aspect ratios, and they reported significant effects on the natural frequency and stress wave propagation of nanocomposite cylinders. Finally, Shams et al. [23] investigated the effects of CNT waviness and aspect ratios on the buckling behavior of FG-CNTRC plates subjected to in-plane loads. They employed a reproducing kernel particle method (RKPM) based on modified FSDT.

In this study, a mesh-free method, based on FSDT, was developed to consider the effects of a two-parameter elastic foundation, CNT waviness, and CNT aspect ratios, on the static and free vibration analyses of nanocomposite plates reinforced by wavy CNTs. Material properties were estimated by a

micromechanical model. Micromechanics' equations cannot capture the scale difference between the nano- and micro-levels. In order to overcome this difficulty, the efficiency parameter was defined and estimated by matching the Young's moduli for the NTRCs obtained by the extended rule of mixture to those obtained by MD simulation. In the mesh-free method, MLS shape functions were used for approximation of the displacement field in the weak form of a motion equation, and the transformation method was used for imposition of essential boundary conditions. This mesh-free method did not increase the calculations against the element-free Galerkin (EFG) method. Four linear types of CNT distributions were considered: uniform distribution, and three kinds of FG distributions. In addition, the other variables examined consisted of plate thickness, and the effects of geometric dimensions, boundary conditions, applied force, waviness index, aspect ratio, volume fraction, and the distribution pattern of CNTs. All of these variables were investigated for their effects on the deflection, stress distributions, and natural frequencies of FG-CNTRC plates.

2. Material Properties of FG-CNTRC Plates

In this paper, FG-CNTRC plates based on the Pasternak elastic foundation were considered with length *a*, width *b*, and thickness *h* (Figure 1). The FG-CNTRC plates were made from a mixture of wavy SWCNTs in an isotropic matrix. The wavy SWCNT reinforcement were either uniformly distributed (UD) or functionally graded (FG) within the plate thickness. To obtain mechanical properties of CNT/polymer composites, a new rule of mixture equation assumed that the fibers were wavy and had uniform dispersion within the polymer matrix. This equation cannot consider the length of fibers, so it can be modified by incorporating an efficiency parameter (η^*) to account for the nanotube aspect ratio (AR) and waviness (*w*) [19]. The effective mechanical properties of the CNTRC plates were obtained based on a micromechanical model according to [6]

$$E_1 = \eta_1 V_{CN} E_{1,\eta^*} + V_m E^m \tag{1}$$

$$\frac{\eta_2}{E_2} = \frac{V_{CN}}{E_{2,\eta^*}} + \frac{V_m}{E^m} \tag{2}$$

$$\frac{\eta_3}{G_{12}} = \frac{V_{CN}}{G_{12,\eta^*}} + \frac{V_m}{G^m} \tag{3}$$

$$\upsilon_{ij} = V_{CN}\upsilon_{ij}^{CN} + V_m \upsilon^m \qquad i, j = 1,2,3 \; and \; i \neq j \tag{4}$$

$$\rho = V_{CN}\rho^{CN} + V_m \rho^m \tag{5}$$

where

$$E_{i,\eta^*} = \eta^* E_i^{CN} \tag{6}$$

$$\eta^* = 1 - \frac{\tanh\left(K.AR/(1+\langle c\rangle)\right)}{K.AR/(1+\langle c\rangle)}, \qquad K = \sqrt{\frac{-2}{1+\upsilon_m}\Big/\left(\frac{E^{CN}}{E^m}\ln(V_{CN})\right)} \tag{7}$$

and where E_i^{CN}, G_{12}^{CN}, υ^{CN}, E_{η^*}, $\langle c\rangle$ and ρ^{CN} are the elasticity modulus, shear modulus, Poisson's ratio, effective reinforcement modulus, the average number of contacts per particle, and density, respectively, of the carbon nanotubes. E^m, G^m, υ^m and ρ^m are corresponding properties for the matrix. V_{CN} and V_m are the fiber (CNT) and matrix volume fractions, and they are related by $V_{CN} + V_m = 1$. The equation η_j ($j = 1,2,3$) showed the CNT efficiency parameters, and the efficiency parameters can be computed by matching the elastic modulus of the CNTRCs observed during the molecular dynamic MD simulation results with the numerical results obtained from the new rule of mixture in Eqs. (1)–(5).

The average number of contacts, $\langle c\rangle$, for the nanotubes is dependent on their aspect ratio [19]

$$\langle c\rangle = w.V_{CN}.\left(4 + \frac{3AR^2}{3AR+2}\right) \tag{8}$$

where the waviness index *w* has been introduced to account for the CNTs' curvature within the real composite. According to the literature [19], the variation of the excluded volume due to nanotubes curvature was investigated by introducing the waviness parameter *w*. The accuracy of this method can be demonstrated through comparison with available literature data.

The profile of the fiber volume fraction variation has important effects on plate behaviors. In this paper, three linear types (FG-V, FG-, and FG-X) were assumed for the distribution of CNT reinforcements along the thickness in FG-CNTRC plates. In addition, a UD of CNTs within the nanocomposite plate of the same thickness, referred to as UD-CNTRCs, were considered as a comparator.

These distributions along the plate's thickness were presented as follows (see Figure 2):

For type V : $$V_{CN} = (\frac{z+h}{h})V_{CN}^* \tag{9}$$

For type X: $$V_{CN} = 2\frac{|z|}{h}V_{CN}^* \tag{10}$$

For type O : $$V_{CN} = 2(1-\frac{|z|}{h})V_{CN}^* \tag{11}$$

For UD: $$V_{CN} = V_{CN}^* \tag{12}$$

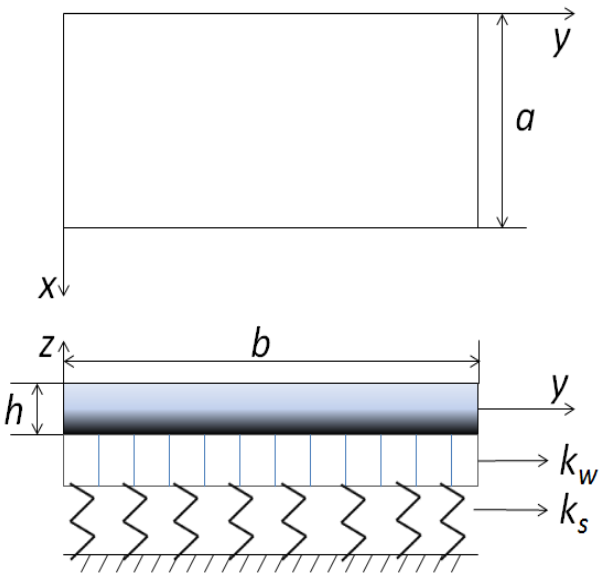

Figure 1. Schematic of the plate resting on a two-parameter elastic foundation.

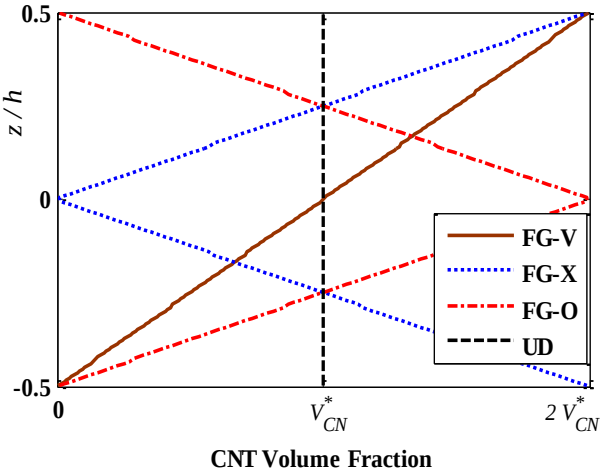

Figure 2. Variation of the nanotubes' volume fraction V_{CN} along the thickness of the plate for different CNT distributions.

where

$$V^*_{CN} = \frac{\rho^m}{\rho^m + (\rho^{CN}/w^{CN}) - \rho^{CN}} \tag{13}$$

and w^{CN} is the mass fraction of the nanotubes.

3. Governing Equations

Based on the FSDT, the displacement components can be defined as

$$\begin{aligned} u(x,y,z) &= u_0(x,y) + z\theta_x(x,y) \\ v(x,y,z) &= v_0(x,y) + z\theta_y(x,y) \\ w(x,y,z) &= w_0(x,y) \end{aligned} \tag{14}$$

where u, v and w are displacements in the x, y, z directions, respectively. The variables u_0, v_0 and w_0 denote midplane displacements, while θ_x and θ_y represent rotations of normal to the midplane about the y-axis and x-axis, respectively. The kinematic relations can be obtained as follows:

$$\begin{bmatrix} \varepsilon_{xx} & \varepsilon_{yy} & \gamma_{xy} \end{bmatrix}^T = \boldsymbol{\varepsilon}_0 + z\boldsymbol{\kappa}, \begin{bmatrix} \gamma_{yz} & \gamma_{xz} \end{bmatrix}^T = \boldsymbol{\gamma}_0 \tag{15}$$

where

$$\boldsymbol{\varepsilon}_0 = \begin{Bmatrix} \partial u_0/\partial x \\ \partial v_0/\partial y \\ \partial u_0/\partial y + \partial v_0/\partial x \end{Bmatrix}, \boldsymbol{\kappa} = \begin{Bmatrix} \partial \theta_x/\partial x \\ \partial \theta_y/\partial y \\ \partial \theta_x/\partial y + \partial \theta_y/\partial x \end{Bmatrix}$$
$$\boldsymbol{\gamma}_0 = \begin{Bmatrix} \partial v/\partial z + \partial w/\partial y \\ \partial u/\partial z + \partial w/\partial x \end{Bmatrix} = \begin{Bmatrix} \varphi_y + \partial w_0/\partial y \\ \varphi_x + \partial w_0/\partial x \end{Bmatrix} \tag{16}$$

The linear constitutive relations of a FG plate can be written as

$$\begin{Bmatrix} \sigma_x \\ \sigma_y \\ \sigma_{xy} \end{Bmatrix} = \begin{bmatrix} Q_{11}(z) & Q_{12}(z) & 0 \\ Q_{12}(z) & Q_{22}(z) & 0 \\ 0 & 0 & Q_{66}(z) \end{bmatrix} or \boldsymbol{\sigma} = \mathbf{Q_b}\boldsymbol{\varepsilon}$$
$$\begin{Bmatrix} \sigma_{yz} \\ \sigma_{xy} \end{Bmatrix} = \alpha(z) \begin{bmatrix} Q_{44}(z) & 0 \\ 0 & Q_{55}(z) \end{bmatrix} or \boldsymbol{\tau} = \alpha(z)\mathbf{Q}_z\boldsymbol{\gamma} \tag{17}$$

in which α denotes the transverse shear correction coefficient, which is suggested as $\alpha = 5/6$ for homogeneous materials. For FGMs, the shear correction coefficient is taken to be $\alpha = 5/(6-(\upsilon_{CN}V_{CN} + \upsilon_m V_m))$ [24].

also where

$$c_{11} = \frac{1-\nu_{23}\nu_{32}}{E_2 E_3 \Delta}, \; c_{22} = \frac{1-\nu_{31}\nu_{13}}{E_1 E_3 \Delta}, \; c_{13} = \frac{\nu_{31}+\nu_{21}\nu_{32}}{E_2 E_3 \Delta}$$
$$c_{33} = \frac{1-\nu_{21}\nu_{12}}{E_1 E_2 \Delta}, \; c_{12} = \frac{\nu_{21}+\nu_{31}\nu_{23}}{E_2 E_3 \Delta}, \; c_{23} = \frac{\nu_{32}+\nu_{12}\nu_{31}}{E_1 E_3 \Delta} \tag{18}$$
$$c_{55} = G_{12}, \; \Delta = \frac{1-\nu_{32}\nu_{23}-\nu_{21}\nu_{12}-\nu_{13}\nu_{31}-2\nu_{32}\nu_{21}\nu_{13}}{E_1 E_2 E_3}$$

In addition, by considering the Pasternak foundation model, total energy of the plate is as

$$U = \frac{1}{2}\int_V \left[\boldsymbol{\varepsilon}^T\boldsymbol{\sigma} + \boldsymbol{\gamma}^T\boldsymbol{\tau} - \rho(z)(\dot{u}^2 + \dot{v}^2 + \dot{w}^2)\right] dV$$
$$+ \frac{1}{2}\int_A \left[k_w w^2 + k_s \left[\left(\frac{\partial w}{\partial x}\right)^2 + \left(\frac{\partial w}{\partial y}\right)^2 \right] \right] dA \tag{19}$$
$$+ \int_A [fw] dA$$

where f is the applied load, and k_w and k_s are coefficients of the Winkler and the Pasternak foundations, respectively. If the foundation was modeled as the linear Winkler foundation, the coefficient k_s in Eq. (19) is zero.

4. Mesh-Free Numerical Analysis

In these analyses, moving least square shape functions introduced by Lancaster and Salkauskas [25] were used for approximation of the displacement vector in the weak form of the motion equation. Displacement vector **d** can be approximated by the MLS shape functions as follows:

$$\hat{\mathbf{d}} = \sum_{i=1}^{N} \phi_i d_i \tag{20}$$

where N is the total number of nodes; $\hat{\mathbf{d}}$ is the virtual nodal values vector, and ϕ_i is the MLS shape function of the node located at $\mathbf{X}(x,y) = \mathbf{X}_i$, and they are defined as follows:

$$\hat{\mathbf{d}} = \left[\hat{u}_i, \hat{v}_i, \hat{w}_i, \hat{\theta}_{xi}, \hat{\theta}_{y_i}\right]^T \tag{21}$$

and

$$\phi_i(\mathbf{X}) = \underbrace{\mathbf{P}^{\mathbf{T}}(\mathbf{X})\left[\mathbf{H}(\mathbf{X})\right]^{-1} W(\mathbf{X}-\mathbf{X}_i)\mathbf{P}(\mathbf{X}_i)}_{(1\times 1)} \tag{22}$$

Where W is the cubic Spline weight function, $\mathbf{P}$ is the base vector, and $\mathbf{H}$ is the moment matrix. The vector and moment matrix can be defined as follows:

$$\mathbf{P}(\mathbf{X}) = [1, x, y]^T \tag{23}$$

$$\mathbf{H}(\mathbf{X}) = \left[\sum_{i=1}^{n} W(\mathbf{X}-\mathbf{X}_i)\mathbf{P}(\mathbf{X}_i)\mathbf{P}^{\mathbf{T}}(\mathbf{X}_i)\right] \tag{24}$$

By using the MLS shape function, Eq. (15) can be written as

$$\boldsymbol{\varepsilon} = \mathbf{B}_m\hat{\mathbf{d}} + z\mathbf{B}_b\hat{\mathbf{d}} \quad , \quad \boldsymbol{\gamma} = \mathbf{B}_s\hat{\mathbf{d}} \tag{25}$$

in which

$$\mathbf{B}_m = \begin{bmatrix} \phi_{i,x} & 0 & 0 & 0 & 0 \\ 0 & \phi_{i,y} & 0 & 0 & 0 \\ \phi_{i,y} & \phi_{i,x} & 0 & 0 & 0 \end{bmatrix}$$

$$\mathbf{B}_b = \begin{bmatrix} 0 & 0 & 0 & \phi_{i,x} & 0 \\ 0 & 0 & 0 & 0 & \phi_{i,y} \\ 0 & 0 & 0 & \phi_{i,y} & \phi_{i,x} \end{bmatrix} \tag{26}$$

$$\mathbf{B}_s = \begin{bmatrix} 0 & 0 & \phi_{i,x} & \phi_i & 0 \\ 0 & 0 & \phi_{i,y} & 0 & \phi_i \end{bmatrix}$$

In addition, for the elastic foundation, $\boldsymbol{\varphi}_w$ and $\mathbf{B}_p$ can be defined as

$$\varphi_p = \begin{bmatrix} 0 & 0 & \phi_i & 0 & 0 \end{bmatrix}$$

$$\mathbf{B}_p = \begin{bmatrix} 0 & 0 & \phi_{i,x} & 0 & 0 \\ 0 & 0 & \phi_{i,y} & 0 & 0 \end{bmatrix} \tag{27}$$

Substitution of Eqs. (17) and (25) into Eq. (19) leads to

$$\begin{aligned} U = {} & \frac{1}{2}\int_A \hat{\mathbf{d}}\int_z \Big[\mathbf{B}_m^T\mathbf{A}\mathbf{B}_m + \mathbf{B}_m^T\overline{\mathbf{B}}\mathbf{B}_b + \mathbf{B}_b^T\overline{\mathbf{B}}\mathbf{B}_m + \\ & \mathbf{B}_b^T\mathbf{D}\mathbf{B}_b + \mathbf{B}_s^T\mathbf{A}_s\mathbf{B}_s\Big]dz\hat{\mathbf{d}}dA \\ & -\frac{1}{2}\int_A \ddot{\hat{\mathbf{d}}}\int_z \left[\mathbf{G}_i^T\overline{\mathbf{M}}\mathbf{G}_j\right]dz\hat{\mathbf{d}}dA + \\ & \frac{1}{2}\int_A \left[\boldsymbol{\varphi}_w^T k_w\boldsymbol{\varphi}_w + \mathbf{B}_p^T k_s\mathbf{B}_p\right]\hat{\mathbf{d}}dA + \frac{1}{2}\int_A \boldsymbol{\varphi}_w^T f dA \end{aligned} \tag{28}$$

in which the components of the extensional stiffness $\mathbf{A}$, bending-extensional coupling stiffness $\overline{\mathbf{B}}$, bending stiffness $\mathbf{D}$, transverse shear stiffness $\mathbf{A}_s$ and also $\mathbf{G}_i$ and $\overline{\mathbf{M}}$, are introduced into the mass matrix. They are defined as

$$(\mathbf{A}, \overline{\mathbf{B}}, \mathbf{D}) = \int_{-h/2}^{h/2} \mathbf{Q}_b(1, z, z^2)dz, \mathbf{A}_s = \alpha\int_{-h/2}^{h/2} \mathbf{Q}_s dz \tag{29}$$

and

$$\mathbf{G}_i = \begin{bmatrix} \phi_i & 0 & 0 & 0 & 0 \\ 0 & \phi_i & 0 & 0 & 0 \\ 0 & 0 & \phi_i & 0 & 0 \\ 0 & 0 & 0 & \phi_i & 0 \\ 0 & 0 & 0 & 0 & \phi_i \end{bmatrix}$$

$$\overline{\mathbf{M}} = \begin{bmatrix} I_0 & 0 & 0 & I_1 & 0 \\ 0 & I_0 & 0 & 0 & I_1 \\ 0 & 0 & I_0 & 0 & 0 \\ I_1 & 0 & 0 & I_2 & 0 \\ 0 & I_1 & 0 & 0 & I_2 \end{bmatrix} \tag{30}$$

where I_0, I_1, and I_2 are the normal, coupled normal-rotary and rotary inertial coefficients, respectively, defined by

$$(I_0, I_1, I_2) = \int_{-h/2}^{h/2} \rho(z)(1, z, z^2)dz \tag{31}$$

The arrays of the bending-extensional coupling stiffness matrix, $\overline{\mathbf{B}}$, are zero for symmetric laminated composites.

Finally, using a derivative with respect to the displacement vector, $\hat{\mathbf{d}}$, the Eq. (28) can be expressed as

$$\mathbf{M}\ddot{\hat{\mathbf{d}}} + \mathbf{K}\hat{\mathbf{d}} = \mathbf{F} \tag{32}$$

in which, $\mathbf{M}$, $\mathbf{K}$, and $\mathbf{F}$ are the mass matrix, stiffness matrix, and force vector, respectively, which are defined as

$$\mathbf{M} = \int_A \mathbf{G}_i^T\overline{\mathbf{M}}\mathbf{G}_j dA \tag{33}$$

$$\mathbf{K} = \mathbf{K}_m + \mathbf{K}_b + \mathbf{K}_s + \mathbf{K}_w + \mathbf{K}_p \tag{34}$$

$$\mathbf{F} = \int_A \boldsymbol{\varphi}_w^T f dA \tag{35}$$

in which, $\mathbf{K}_m$, $\mathbf{K}_b$, and $\mathbf{K}_s$ are the stiffness matrices of the extensional, bending-extensional, and bending, respectively, while $\mathbf{K}_w$ and $\mathbf{K}_p$ are the stiffness matrices that represented the Winkler and Pasternak elastic foundations. They are defined as

$$\begin{aligned} \mathbf{K}_m &= \int_A \left[\mathbf{B}_m^T\mathbf{A}\mathbf{B}_m + \mathbf{B}_m^T\overline{\mathbf{B}}\mathbf{B}_b + \mathbf{B}_b^T\overline{\mathbf{B}}\mathbf{B}_m\right]dA \\ \mathbf{K}_b &= \int_A \mathbf{B}_b^T\mathbf{D}\mathbf{B}_b dA \ , \ \mathbf{K}_s = \int_z \mathbf{B}_s^T\mathbf{A}_s\mathbf{B}_s dA \end{aligned} \tag{36}$$

$$\mathbf{K}_w = \int_A \boldsymbol{\varphi}_w^T k_w\boldsymbol{\varphi}_w dA \ , \ \mathbf{K}_p = \int_A \mathbf{B}_p^T k_s\mathbf{B}_p dA \tag{37}$$

For numerical integration, the problem domain is discretized to a set of background cells with gauss points inside each cell. Then, the global stiffness matrix $\mathbf{K}$ is obtained numerically by sweeping all gauss points.

Imposition of essential boundary conditions in the system of Eq. (32) was not possible because MLS shape functions do not satisfy the Kronecker delta property. In this work, the transformation method is used for imposition of essential boundary conditions. For this purpose, a transformation matrix is formed by establishing the relationship between nodal displacement vector $\mathbf{d}$ and virtual displacement vector $\hat{\mathbf{d}}$.

$$\mathbf{d} = \mathbf{T}\hat{\mathbf{d}} \tag{38}$$

$\mathbf{T}$ is the transformation matrix that is a ($5N \times 5N$) matrix defined as

$\mathbf{T}_i =$

$$\begin{bmatrix} \phi_1(x_1)\times\mathbf{I}_{(5\times5)} & \phi_1(x_2)\times\mathbf{I}_{(5\times5)} & . \; . & \phi_1(x_N)\times\mathbf{I}_{(5\times5)} \\ \phi_2(x_1)\times\mathbf{I}_{(5\times5)} & \phi_2(x_2)\times\mathbf{I}_{(5\times5)} & . \; . & \phi_2(x_N)\times\mathbf{I}_{(5\times5)} \\ . & . & . \; . & . \\ . & . & . \; . & . \\ \phi_N(x_1)\times\mathbf{I}_{(5\times5)} & \phi_N(x_2)\times\mathbf{I}_{(5\times5)} & . \; . & \phi_N(x_N)\times\mathbf{I}_{(5\times5)} \end{bmatrix} \tag{39}$$

where $\mathbf{I}_{(5\times5)}$ is an identity matrix of size 5. By using Eq. (38), the system of linear Eq. (32) can be rearranged to

$$\hat{\mathbf{M}}\ddot{\mathbf{d}} + \hat{\mathbf{K}}\mathbf{d} = \hat{\mathbf{F}} \tag{40}$$

where

$$\hat{\mathbf{M}} = \mathbf{T}^{-T}\mathbf{M}\mathbf{T}^{-1}, \hat{\mathbf{K}} = \mathbf{T}^{-T}\mathbf{K}\mathbf{T}^{-1}, \hat{\mathbf{F}} = \mathbf{T}^{-T}\mathbf{F} \tag{41}$$

Now the essential BCs. can be enforced within the modified equations system in Eq. (40) easily, like the FEM.

For a static problem, the mass matrix is eliminated, and Eq. (40) is changed to

$$\hat{\mathbf{K}}\mathbf{d} = \hat{\mathbf{F}} \tag{42}$$

Therefore, the stress and displacement fields of the plate can be derived, solving this equation system. Additionally, in the absence of external forces, Eq. (40) is simplified as follows:

$$\hat{\mathbf{M}}\ddot{\mathbf{d}} + \hat{\mathbf{K}}\mathbf{d} = 0 \tag{43}$$

Thus, the natural frequencies and mode shapes of the plate are determined by solving this eigenvalue problem.

Table 1. Comparisons of Young's moduli for polymer/CNT composites reinforced by (10,10) SWCNT at T_0 = 300 K [7].

V_{CN}^*	MD		Extended rule of mixture			
	E_1 (GPa)	E_2 (GPa)	E_1 (GPa)	η_1	E_2 (GPa)	η_2
0.12	94.6	2.9	94.78	0.137	2.9	1.022
0.17	138.9	4.9	138.68	0.142	4.9	1.626
0.28	224.2	5.5	224.50	0.141	5.5	1.585

5. Results and Discussions

In the following simulations, static and vibration behaviors of the nanocomposite plates are characterized as FG plates reinforced by wavy CNTs. The polymer (methyl-methacrylate), referred to as PMMA, was selected as the matrix material. The relevant material properties for CNTs and PMMA are as follows [7]:

$E^m = 2.5GPa$, $\rho^m = 1150\ Kg/m^3$ and $\upsilon^m = 0.34$

for PMMA. For (10,10) SWCNTs

$E_1^{CN} = 5.6466$, $E_2^{CN} = 7.0800$, $G_{12}^{CN} = 1.9445TPa$,

$\rho^{CN} = 1400\ Kg/m^3$ and $\upsilon_{12}^{CN} = 0.175$

and the material properties of the nanocomposite are derived from Eqs. (1)–(6) with respect to $\eta_3 = 0.7\eta_2$ [26] and the values in Table 1 [14]. The accuracy of this method was investigated by comparison with experimental results [20-22].

In this work, the static and free vibration analyses were presented to investigate the mechanical characteristics of FG-CNTRC plates using several numerical examples. The plates were assumed to be resting on two-parameter elastic foundations, and the developed mesh-free method was used. At first, the convergence and accuracy of the mesh-free method on the static and vibrational behaviours of the plates were examined by a comparison between the results and reported results in the literature concerning homogeneous FGMs and straight CNTRC plates. Then, new mesh-free results on the static and free vibration characteristics of the wavy CNTRC plates on the elastic foundation were reported.

In all examples of CNTRC plates, the foundation parameters were presented in the non-dimensional form of $K_w = k_w a^4/D$ and $K_s = k_s a^2/D$, in which $D = E_m h^3/12(1-\upsilon_m^2)$ was the reference bending rigidity of the plate. In addition, the non-dimensional deflections and the natural frequencies of the CNTRC plates are defined as [27]

$$\hat{q} = 10^2 E_m h^3 q / f_0 a^4 \tag{44}$$

$$\hat{\omega} = \omega h\sqrt{\rho/E_m} \tag{45}$$

where, f_0 is the value of applied (concentrated or uniform) load, and q is the central deflection.

5.1. Validation of models

In the first example, consider a simply supported homogeneous square plate under uniformly distributed load f_0. The convergence of the developed mesh-free method in a central non-dimensional deflection $\hat{q}$ of the plate with h/ac= 0.02, is shown in Figure 3. The applied mesh-free method has an excellent convergence and agreement with the exact results reported by Akhras et al. [28] in the bending analysis of the plate. The deflections of this plate for

various values of h/a (=0.1, 0.05, 0.02 and 0.01) are listed in Table 2. The accuracy of the applied method was evident by comparison with exact [28] and other reported results [27,29,30]. Figure 3 and Table 2 results show that by using an 11 × 11 node arrangement, the applied method provided more accuracy than FEM.

The bending analysis of the FG nanocomposite plate reinforced by straight CNT and without an elastic foundation was also validated. Consider a square clamped FG-CNTRC plate with a CNT volume fraction $V_{CN}^{*}=0.17$, and values of b/h at 50, 20, and 10. Table 3 shows good agreement between the results of the applied mesh-free method, and the FEM reported results by Zhu et al. [8] for both UD and FG nanocomposite reinforced by straight CNTs.

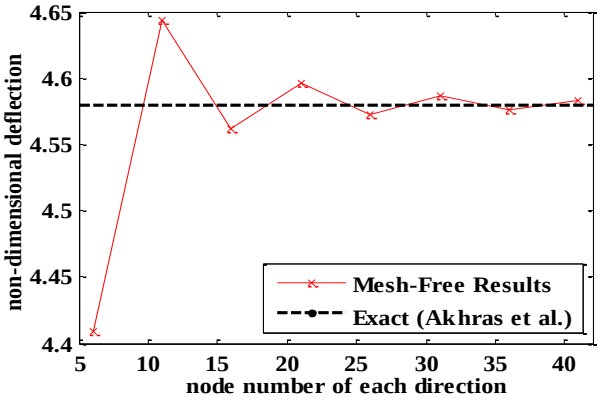

Figure 3. Convergence of the central non-dimensional deflection $\hat{q}$, for different numbers of nodes in each direction (data comparision with Akhares et al. [28]).

Table 2. Comparison of the central non-dimensional deflection $\hat{q}$ in simply supported square plates subjected to uniformly distributed load.

h/a	Method	Non-dimensional Deflection
0.1	Present	4.7864
	Exact [28]	4.7910
	Ferreira et al. [29]	4.7866
	Ferreira et al. [27]	4.7912
	FEM (Reddy [30])	4.7700
0.05	Present	4.6274
	Exact [28]	4.6250
	Ferreira et al. [29]	4.6132
	Ferreira et al. [27]	4.6254
	FEM (Reddy [30])	4.5700
0.02	Present	4.5829
	Exact [28]	4.5790
	Ferreira et al. [29]	4.5753
	Ferreira et al. [27]	4.5788
	FEM (Reddy [30])	4.4960
0.01	Present	4.5765
	Exact [28]	4.5720
	Ferreira et al. [29]	4.5737
	Ferreira et al. [27]	4.5716
	FEM (Reddy [30])	4.4820

Table 3. Comparison of the central non-dimensional deflection $\hat{q}$, in clamped square plates reinforced by straight CNTs.

b/h	UD		FG-X	
	Mesh-Free (35×35)	Zhu et al. [8]	Mesh-Free (35×35)	Zhu et al. [8]
50	0.1690	0.1698	0.1213	0.1223
20	8.309×10^{-2}	8.561×10^{-2}	7.039×10^{-3}	7.290×10^{-3}
10	1.353×10^{-3}	1.412×10^{-3}	1.261×10^{-3}	1.318×10^{-3}

In the second stage of validation, consider a simply supported FGM square plate as reported in Thai and Choi [4] in which the material properties of plate are varied as follows:

$$P(z)=P_b+(P_t-P_b)(\frac{1}{2}+\frac{z}{h})^n \quad (46)$$

where P is an indicator for the material properties of a plate that were used in place of the modulus elasticity, E, Poisson's ratio, υ, and density, ρ. Additionally, n is the volume fraction exponent, and the subscripts b and t represent the bottom and top constituents, respectively. The convergence of the applied mesh-free method in a non-dimensional fundamental frequency $\hat{\omega}$, for plates resting on a Winkler-Pasternak elastic foundation with h/a = 0.2, K_w = 100, K_s = 100, and a volume fraction exponent of n = 1, are shown in Figure 4. This figure also shows that by using only a 5 × 5 node arrangement, the applied method had very good accuracy and agreement with the results reported by Thai and Choi [4] for FGM (n = 1) plates. The non-dimensional fundamental frequencies for this plate are presented in Table 4, using various values of h/a that equal 0.05, 0.1, and 0.2, and including elastic foundation coefficients. This table reveals that the applied method had very good accuracy and agreement with the reported results, especially for thinner plates.

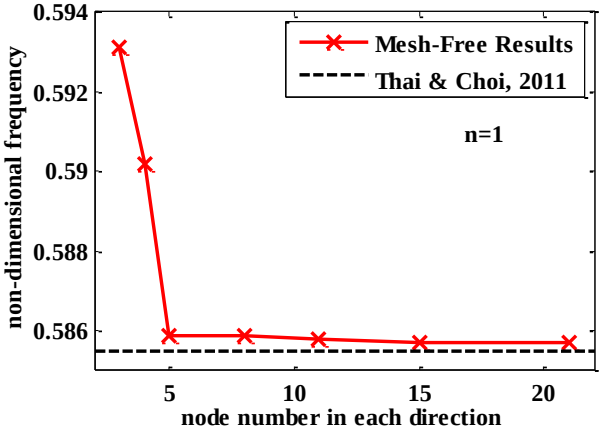

Figure 4. Convergence of the non-dimensional fundamental frequency $\hat{\omega}$, for the FGM plates with n=1, h/a=0.2, K_w=100, K_s=100 for different numbers of nodes in each direction (data comparison with Thai and Choi [4]).

Table 4. Comparison of the fundamental frequency, $\hat{\omega}$, in simply supported square FGM plates.

K_w	K_s	h/a	Method	n=0	n=1
0	0	0.05	Present	0.0291	0.0222
			Baferani et al. [31]	0.0291	0.0227
			Thai & Choi [4]	0.0291	0.0222
		0.1	Present	0.1135	0.0869
			Baferani et al. [31]	0.1134	0.0891
			Thai & Choi [4]	0.1135	0.0869
		0.2	Present	0.4167	0.3216
			Baferani et al. [31]	0.4154	0.3299
			Thai & Choi [4]	0.4154	0.3207
100	100	0.05	Present	0.0411	0.0384
			Baferani et al. [31]	0.0411	0.0388
			Thai & Choi [4]	0.0411	0.0384
		0.1	Present	0.1618	0.1519
			Baferani et al. [31]	0.1619	0.1542
			Thai & Choi [4]	0.1619	0.1520
		0.2	Present	0.6167	0.5857
			Baferani et al. [31]	0.6162	0.5978
			Thai & Choi [4]	0.6162	0.5855

Table 5. Comparison of the fundamental frequency $\hat{\omega}$, in simply supported square plates reinforced by straight CNTs

b/h	UD			FG-X		
	Mesh-Free (31×31)	FEM (31×31)	Zhu et al. [8]	Mesh-Free (31×31)	FEM (31×31)	Zhu et al. [8]
10	17.0010	17.0189	16.815	18.5240	18.5382	18.278
20	21.5053	21.541	21.456	24.8639	24.8973	24.764
50	23.6323	23.6791	23.697	28.3400	28.3891	28.413

Finally, consider square simply supported FG-CNTRC plates with a CNT volume fraction $V_{CN}^{*}=0.17$, and values of b/h equal to 50, 20, and 10. Table 5 shows a good agreement between the non-dimensional fundamental frequency $\hat{\omega}$ of the applied mesh-free method, FEM, and FEM reported results by Zhu et al. [8], for both UD and FG nanocomposites reinforced by straight CNTs.

5.2. Static analysis of FG-CNTRC plates

Consider square clamped nanocomposite plates reinforced by wavy CNTs subjected to uniformed distribution load of f_0 = -1e5, resting on a Pasternak foundation with the values K_w = 100, K_s = 10, and h/a = 0.1. Table 6 shows the central non-dimensional deflection $\hat{q}$, for the plates for different types of CNT distributions and various values of CNT volume fraction V_{CN}^{*}, aspect ratio, and waviness index. The deflection parameter was decreased by increasing the CNT volume fraction, CNT aspect ratio, and by decreasing the waviness index. Table 6 reveals that the CNT waviness had the biggest effect (even more than the CNT volume fraction), and CNT aspect ratio had the smallest effect (especially at its higher values) on the bending behaviors of FG-CNTRC plates. Additionally, in more cases, the FG-X and FG-O types of CNTRC plates have the minimum and maximum values for non-dimensional deflection, respectively.

Table 6. Central non-dimensional deflections $\hat{q}$, in clamped square FG-CNTRC plates, with the values K_{wv} = 100, K_{sv} = 10, f_{0v} = v-1e5, and h/a = 0.1

V_{CN}^{*}	w	AR	UD	FG-V	FG-X	FG-O
0.12	0	100	0.5470	0.5825	0.5010	0.6369
		500	0.4984	0.5212	0.4726	0.5530
		1000	0.4949	0.5165	0.4705	0.5465
	0.425	100	0.9536	0.9623	0.9470	0.9669
		500	0.9221	0.9183	0.9235	0.9046
		1000	0.9172	0.9102	0.9198	0.8928
0.17	0	100	0.3459	0.3691	0.3101	0.4103
		500	0.3145	0.3295	0.2929	0.3544
		1000	0.3122	0.3263	0.2915	0.3500
	0.425	100	0.6653	0.6595	0.6427	0.6765
		500	0.6603	0.6501	0.6402	0.6575
		1000	0.6592	0.6471	0.6396	0.6524
0.28	0	100	0.2864	0.2936	0.2512	0.3259
		500	0.2702	0.2713	0.2437	0.2916
		1000	0.2689	0.2695	0.2430	0.2889
	0.425	100	0.6377	0.6219	0.5841	0.6595
		500	0.6360	0.6141	0.5826	0.6439
		1000	0.6356	0.6118	0.5823	0.6399

Despite increased CNT volume fractions from $V_{CN}^{*}=0.17$ to $V_{CN}^{*}=0.28$, deflection can be reduced by using a proper CNT distribution. Also, Figure 5 shows variations in the normalized deflection of the plates versus the waviness index for the FG-X type of distribution of CNTs, AR = 1000, and various values of CNT volume fractions. Increasing the CNT volume decreased the deflection values for the plates with straight or wavy CNTs. In most cases, the deflection was increased with an increased waviness index.

To investigate the effect of the type of applied force on bending behaviors of these plates, consider square clamped nanocomposite plates subjected to a uniformed distribution load or a concentrated force with the same values of f_0 = -1e5, with h/a = 0.1, AR = 1000, and $V_{CN}^{*}=0.17$. Table 7 shows the non-dimensional deflection of these plates for elastic foundation parameters of K_w = 0 or 100, and K_s = 0 or 100, and for w = 0 or 0.425. The table shows that the concentrated forces and the wavy type of CNTs dramatically increased the deflection of the plate. Additionally, in wavy nanocomposite plates, UD distribution caused the largest value in the deflection parameter. Elastic foundations decreased the deflection of all plates.

The effect of essential boundary conditions on the deflection of square and rectangular FG-CNTRC plates, subjected to uniform distributed force f_0 = -1e5, with the values K_w = 100, K_s = 10, w = 0.425, AR = 1000, and $V_{CN}^{*}=0.17$, was investigated in Table 8, where C, S, and F represented clamped, simply supported, and free edges. The table shows that the clamped plates have the smallest values of deflection, while the simply supported plates have the largest ones. Evidently, the deflection parameter

was dramatically increased by increasing the ratio of a/b from 1 to 3 because the plate nearly reveals the beam's manners. Increasing the thickness of the plate increased the non-dimensional deflections $\hat{q}$, because of their definition, but the deflection was decreased by increasing the plate's thickness.

In the next example, the elastic foundation coefficients of FG-CNTRC plates, subjected to uniform distributed load, are investigated.

Figures 6 and 7 demonstrate the non-dimensional deflection of FG-CNTRC plates versus the Winkler coefficient K_w, and shear coefficient K_s, respectively. These plates are square and clamped using an FG-X type CNT distribution, and with the values f_0 =-1e5, w = 0.425, AR = 1000, V_{CN}^{*} =0.17, and h/a = 0.1. These figures revealed that increased foundation coefficients decreased the plates' deflection, but the shear coefficient had a larger effect, particularly in the smaller values of the Winkler coefficient.

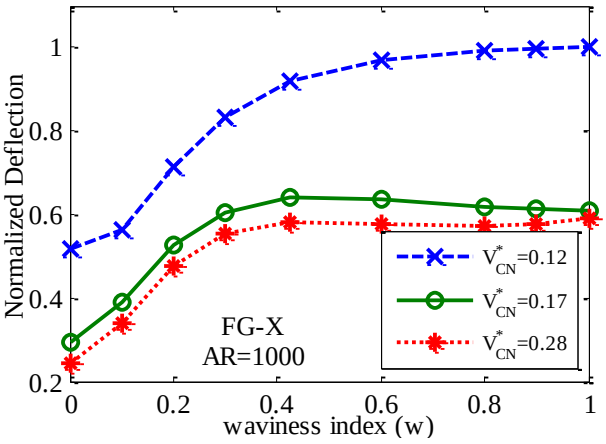

Figure 5. Central normalized deflections $\hat{q}$, versus the waviness index in clamped square X-CNTRC plates, with the values AR = 1000, K_w = 100, K_s =10, f_0 =-1e5, and h/a = 0.1.

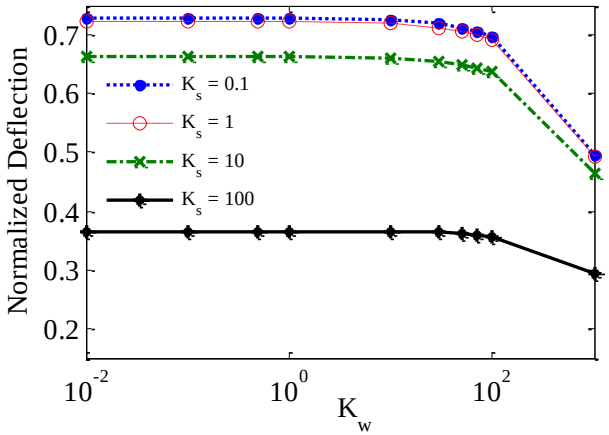

Figure 6. Central non-dimensional deflections $\hat{q}$, versus K_w in square clamped X-CNTRC plates, with the values f_0 = -1e5, w = 0.425, AR = 1000, V_{CN}^{*} = 0.17, and h/a = 0.1.

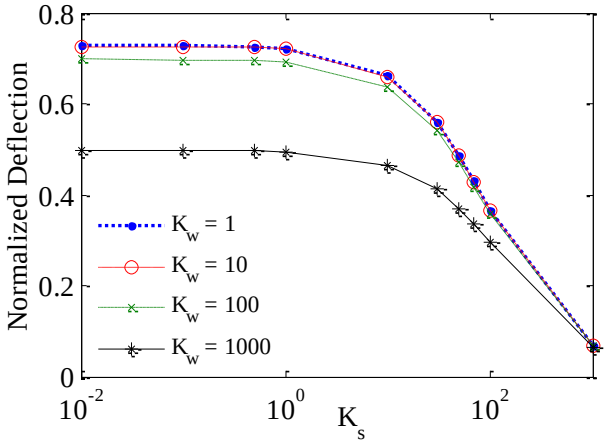

Figure 7. Central non-dimensional deflections $\hat{q}$, versus K_s in square clamped X-CNTRC plates, with the values f_0 = -1e5, w = 0.425, AR = 1000, V_{CN}^{*} = 0.17, and h/a = 0.1.

Table 7. Central non-dimensional deflections $\hat{q}$, in clamped, square FG-CNTRC plates with the values AR = 1000, V_{CN}^{*} = 0.17, and h/a = 0.1

K_w	K_s	w	*Uniform distributed force*				*Concentrated force*			
			UD	FG-V	FG-X	FG-O	UD	FG-V	FG-X	FG-O
0	0	0	0.3334	0.3496	0.3100	0.3768	3.4612	3.4922	3.3146	3.6275
		0.425	0.7595	0.7435	0.7335	0.7505	5.1815	5.0946	5.0442	5.1396
100	100	0	0.2267	0.2341	0.2157	0.2459	2.5988	2.6083	2.5241	2.6687
		0.425	0.3648	0.3611	0.3589	0.3626	3.1911	3.1607	3.1464	3.1730

Table 8. Central non-dimensional deflections $\hat{q}$, in CNTRC plates with K_w = 100, K_s = 10, f_0 = -1e5, w = 0.425, AR = 1000, and V_{CN}^{*} = 0.17

h/a	b/a	CCCC		CSCF		SSSS	
		UD	FG-X	UD	FG-X	UD	FG-X
0.05	1	0.5545	0.5345	0.9102	0.8332	1.4703	1.4081
	3	0.9980	1.0477	6.6235	6.5770	3.0439	3.1287
0.1	1	0.6592	0.6396	1.0440	0.9706	1.5315	1.4710
	3	1.1474	1.1933	6.6585	6.6150	3.1014	3.1826
0.2	1	1.0153	0.9959	1.4961	1.4344	1.7566	1.7017
	3	1.6705	1.7029	6.7670	6.7315	3.3130	3.3814

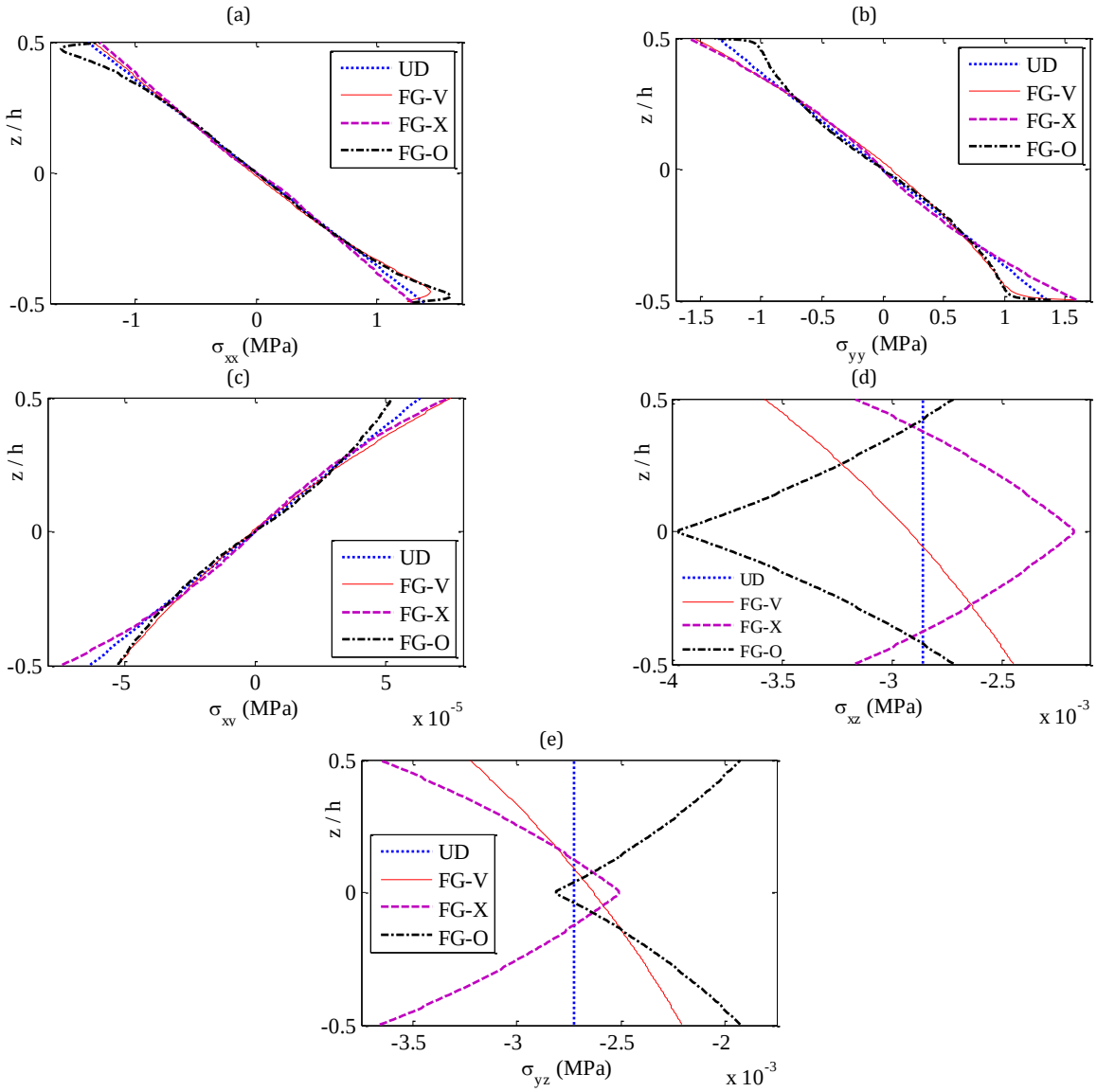

Figure 8. (a) σ_{xx}, (b) σ_{yy}, (c) σ_{xy}, (d) σ_{xz}, and (e) σ_{yz}, square FG-CNTRC plates clamped along the thickness, with the values K_w = 100, K_s = 10, f_0 = -1e5, w = 0.425, AR = 1000, $V_{CN}^{*} = 0.17$, and h/a = 0.1.

Finally, stress distributions of square nanocomposite plates clamped along the thickness of the plate are illustrated in Fig. 8 for plates with the values K_w = 100, K_s = 10, f_0 = -1e5, w= 0.425, AR = 1000, $V_{CN}^{*} = 0.17$, and h/a = 0.1. CNT distribution had a significant effect on the stress distribution, and the values of normal stresses were more than the shear stress values.

5.3. Free vibration analysis of FG-CNTRC plates

Consider square clamped nanocomposite plates reinforced by wavy CNTs resting on a Pasternak foundation with the values K_w = 100, K_s = 10, and h/a = 0.1.

Table 9 shows the frequency parameter $\hat{\omega}$, for the plates with different types of CNT distribution, and various values of CNT volume fraction V_{CN}^{*}, aspect ratio, and waviness index. The frequency parameter was increased by increasing the CNT volume fraction and CNT aspect ratio, and by decreasing the waviness index. This table reveals that the CNT waviness had the largest effect (even more than the CNT volume fraction), while the CNT aspect ratio had the smallest effect, particularly in its larger values, on the frequencies of FG-CNTRC plates. With the FG-X and FG-O CNT distribution types, the CNTRC plates showed the maximum and minimum values in the frequency parameter, respectively.

Table 9. Non-dimensional fundamental frequency $\hat{\omega}$, in clamped square plates with the values K_w = 100, K_s = 10, and h/a = 0.1

V_{CN}^*	w	AR	UD	FG-V	FG-X	FG-O
0.12	0	100	16.4091	15.9619	17.0870	15.3134
		500	17.1010	16.7771	17.5304	16.3236
		1000	17.1542	16.8447	17.5649	16.4092
	0.425	100	12.6534	12.5975	12.6980	12.5673
		500	12.8625	12.8890	12.8559	12.9806
		1000	12.8962	12.9446	12.8811	13.0626
0.17	0	100	20.5661	19.9943	21.6430	19.0273
		500	21.4565	21.0409	22.1945	20.3333
		1000	21.5275	21.1309	22.2398	20.4479
	0.425	100	15.1032	15.1681	15.3568	14.9845
		500	15.1631	15.2817	15.3910	15.2004
		1000	15.1757	15.3169	15.3990	15.2597
0.28	0	100	22.2456	22.0692	23.7155	20.9892
		500	22.8240	22.8535	24.0347	22.0557
		1000	22.8716	22.9211	24.0630	22.1479
	0.425	100	15.2542	15.4474	15.9190	15.0170
		500	15.2785	15.5516	15.9444	15.2017
		1000	15.2839	15.5810	15.9495	15.2491

In the next example, the effects of the elastic foundation coefficients were investigated on the square clamped nanocomposite plates, with values of AR = 1000, $V_{CN}^* = 0.17$, and h/a = 0.1.

Table 10. Non-dimensional fundamental frequency $\hat{\omega}$, in clamped square plates with the values AR = 1000, $V_{CN}^* = 0.17$, and h/a = 0.1

K_w	K_s	w	UD	FG-V	FG-X	FG-O
0	0	0	20.8588	22.4490	21.5944	19.7404
		0.425	14.1890	14.3402	14.4291	14.2778
	100	0	24.9941	24.6572	25.6049	24.0851
		0.425	19.9084	20.0160	20.0734	19.9774
100	0	0	21.0740	20.6684	20.8023	19.9675
		0.425	14.5020	14.6499	14.7370	14.5890
	100	0	25.1741	24.8396	25.7806	24.2717
		0.425	20.1328	20.2393	20.2960	20.2012

Table 10 displays the non-dimensional frequency parameters of these plates for elastic foundation parameter values of K_w= 0 or 100, K_s=0 or 100, and w = 0 or 0.425. This table reveals that the elastic foundation increased the frequency parameters of the plates, but the shear coefficient had a larger effect than the Winkler coefficient.

Table 11. Non-dimensional fundamental frequency $\hat{\omega}$, in CNTRC plates with K_w = 100, K_s = 10, w = 0.425, AR = 1000, and $V_{CN}^* = 0.17$

h/a	b/a	CCCC		CSCF		SSSS		FFFF	
		UD	FG-X	UD	FG-X	UD	FG-X	UD	FG-X
0.05	1	16.7546	17.0581	11.1890	11.7203	10.1382	10.3576	4.4405	4.4398
	3	11.5422	11.3124	3.8505	3.8805	6.6867	6.6199	3.1906	3.1916
0.1	1	15.1757	15.3990	10.4140	10.8249	9.8516	10.0493	4.4217	4.4207
	3	10.7021	10.5348	3.8350	3.8630	6.5908	6.5289	3.1893	3.1902
0.2	1	11.9603	12.0720	8.6479	8.8533	9.0085	9.1504	4.3500	4.3482
	3	8.7779	8.7176	3.3025	3.3217	3.6705	3.6903	3.1843	3.1850

Finally, the effects of the essential boundary conditions on the frequencies of square and rectangular FG-CNTRC plates, with the values K_w = 100, K_s = 10, w = 0.425, AR = 1000, and $V_{CN}^* = 0.17$, were investigated and are displayed in Table 11. This table reveals that the clamped plates had the largest values for the frequency parameters, while the free plates had the smallest values. The frequency parameter values for square plates were also more than the values for the rectangular plates.

6. Conclusions

In this paper, a mesh-free method, based on FSDT, was developed to analyze static and free vibration of FG nanocomposite plates, reinforced by wavy CNTs resting on a Pasternak elastic foundation. Material properties of the CNTRC plates were assumed to be graded within the thickness of the plate and estimated by an extended rule of mixture. Therefore, the effects of the aspect ratios, waviness index, distribution pattern, volume fraction of CNTs, boundary conditions, and dimensions of the plates, were investigated regarding the static and vibrational behaviors of the FG-CNTRC plates.

The following results were obtained:

- The developed mesh-free method had an excellent convergence and accuracy in both the static and free vibration analysis of FG-CNTRC plates.
- The waviness and distribution pattern of CNTs had a significant effect on the static and vibrational behaviors of FG-CNTRC plates, even more than the effect of the CNT volume fractions.
- The aspect ratio of CNTs had a small effect on the static and vibrational behaviors of FG-CNTRC plates, particularly at its larger values.
- In most CNT distributions, FG-X and FG-O showed the best and worst reinforcement behaviors, respectively.
- With the same values, a concentrated force led to more deflection than a uniform distributed force.
- The shear coefficient of an elastic foundation had a larger effect on the mechanical behaviors of FG-CNTRC plates than the Winkler coefficient.
- The values of normal stresses increased more than the values of shear stresses.

References

[1] Iijima S, Ichihashi T. Single-shell carbon nanotubes of 1-nm diameter. *Nature,* 1993; 363: 603-5.

[2] Thostenson ET, Ren Z, Chou T-W. Advances in the science and technology of carbon nanotubes and their composites: a review. *Compos Sci Technol,* 2001; 61: 1899–912.

[3] Fiedler B, Gojny FH, Wichmann MHG, Nolte MCM, Schulte K. Fundamental aspects of nano-reinforced composites. *Compos Sci Technol,* 2006; 66: 3115–25.

[4] Thai HT, Choi DH. A refined plate theory for functionally graded plates resting on elastic foundation. *Compos Sci Technol,* 2011; 71: 1850–1858.

[5] Meguid SA, Sun Y. On the tensile and shear strength of nano-reinforced composite interfaces. *Mater Des*, 2004; 25: 289–96.

[6] Shen HS. Nonlinear bending of functionally graded carbon nanotube- reinforced composite plates in thermal environments. *Compos Struct*, 2009; 91: 9-19.

[7] Shen HS. Postbuckling of nanotube-reinforced composite cylindrical shells in thermal environments, Part I: Axially-loaded shells. *Compos Struct,* 2011; 93: 2096-108.

[8] Zhu P, Lei ZX, Liew KM. Static and free vibration analyses of carbon nanotube-reinforced composite plates using finite element method with first order shear deformation plate theory, *Compos Struct*, 2012; 94: 1450–1460.

[9] Alibeigloo A. Static analysis of functionally graded carbon nanotube-reinforced composite plate embedded in piezoelectric layers by using theory of elasticity. *Compos Struct,* 2013; 95: 612–22.

[10] Malekzadeh P, Zarei AR. Free vibration of quadrilateral laminated plates with carbon nanotube reinforced composite layers, *Thin-Walled Struct,* 2014; 82: 221–232.

[11] Alibeigloo A, Liew KM. Thermoelastic analysis of functionally graded carbon nanotube-reinforced composite plate using theory of elasticity. *Compos Struct,* 2013; 106: 873–881.

[12] Moradi-Dastjerdi R, Payganeh G, Malek-Mohammadi H. Free Vibration Analyses of Functionally Graded CNT Reinforced Nanocomposite Sandwich Plates Resting on Elastic Foundation. *J Solid Mech,* 2015; 7: 158-172.

[13] Moradi-Dastjerdi R, Foroutan M, Pourasghar A. Dynamic analysis of functionally graded nanocomposite cylinders reinforced by carbon nanotube by a mesh-free method. *Mater Des,* 2013; 44: 256–66.

[14] Moradi-Dastjerdi R, Foroutan M, Pourasghar A, Sotoudeh-Bahreini R. Static analysis of functionally graded carbon nanotube-reinforced composite cylinders by a mesh-free method. *J Reinf Plast Comp,* 2013; 32: 593-601.

[15] Moradi-Dastjerdi R, Pourasghar A, Foroutan M. The effects of carbon nanotube orientation and aggregation on vibrational behavior of functionally graded nanocomposite cylinders by a mesh-free method. *Acta Mech,* 2013; 224: 2817-2832.

[16] Lei ZX, Liew KM, Yu JL. Free vibration analysis of functionally graded carbon nanotube-reinforced composite plates using the element-free kp-Ritz method in thermal environment. *Compos Struct,* 2013; 106: 128–138.

[17] Zhang LW, Lei ZX, Liew KM. An element-free IMLS-Ritz framework for buckling analysis of FG–CNT reinforced composite thick plates resting on Winkler foundations. *Eng Anal Bound Elem,* 2015; 58: 7–17.

[18] Zhang LW, Song ZG, Liew KM. Nonlinear bending analysis of FG-CNT reinforced composite thick plates resting on Pasternak foundations using the element-free IMLS-Ritz method. *Compos Struct,* 2015; 128: 165–175.

[19] Martone FG, Antonucci V, Giordano M, et al. The effect of the aspect ratio of carbon nanotubes on their effective reinforcement modulus in an epoxy matrix. *Compos Sci Technol,* 2011; 71: 1117–1123.

[20] Jam JE, Pourasghar A, Kamarian S. The effect of the aspect ratio and waviness of CNTs on the vibrational behavior of functionally graded nanocomposite cylindrical panels. *Polymer Compos,* 2012; 33: 2036-44.

[21] Moradi-Dastjerdi R, Pourasghar A, Foroutan M, Bidram M. Vibration analysis of functionally graded nanocomposite cylinders reinforced by wavy carbon nanotube based on mesh-free method. *J Compos Mater,* 2014; 48: 1901-13.

[22] Moradi-Dastjerdi R, Pourasghar A. Dynamic analysis of functionally graded nanocomposite cylinders reinforced by wavy carbon nanotube under an impact load. *J Vib Control,* 2016: 22, 1062-1075.

[23] Shams S, Soltani B. The Effects of Carbon Nanotube Waviness and Aspect Ratio on the Buckling Behavior of Functionally Graded Nanocomposite Plates Using a Meshfree Method. *Polymer Compos,* 2015; DOI 10.1002/pc.23814.

[24] Efraim E and Eisenberger M. Exact vibration analysis of variable thickness thick annular isotropic and FGM plates. *J Sound Vib,* 2007; 299: 720–38.

[25] Lancaster P, Salkauskas K. Surface Generated by Moving Least Squares Methods. *Math Comput,* 1981; 37: 141-58.

[26] Song YS, Youn JR. Modeling of effective elastic properties for polymer based carbon nanotube composites. *Polym,* 2006; 47: 1741–8.

[27] Ferreira AJM, Castro LMS, Bertoluzza S. A high order collocation method for the static and vibration analysis of composite plates using a first-order theory. *Compos Struct,* 2009; 89: 424–432.

[28] Akhras G, Cheung MS, Li W. Finite strip analysis for anisotropic laminated composite plates using higher-order deformation theory. *Compos Struct,* 1994; 52: 471–7.

[29] Ferreira AJM, Roque CMC, Martins PALS. Analysis of composite plates using higher-order shear deformation theory and a finite point formulation based on the multiquadric radial basis function method. *Compos Part B,* 2003; 34: 627–36.

[30] Reddy JN. **Introduction to the finite element method.** New York: McGraw-Hill; 1993.

[31] Baferani AH, Saidi AR, Ehteshami H. Accurate solution for free vibration analysis of functionally graded thick rectangular plates resting on elastic foundation. *Compos Struct,* 2011; 93: 1842–53.